

GeoDiff3D: Self-Supervised 3D Scene Generation with Geometry-Constrained 2D Diffusion Guidance

HAOZHI ZHU, Nanjing University, China
 MIAOMIAO ZHAO*, Nanjing University, China
 DINGYAO LIU, Nanjing University, China
 RUNZE TIAN, Nanjing University, China
 YAN ZHANG[†], Nanjing University, China
 JIE GUO[‡], Nanjing University, China
 FENGGUEN YU, Simon Fraser university, China

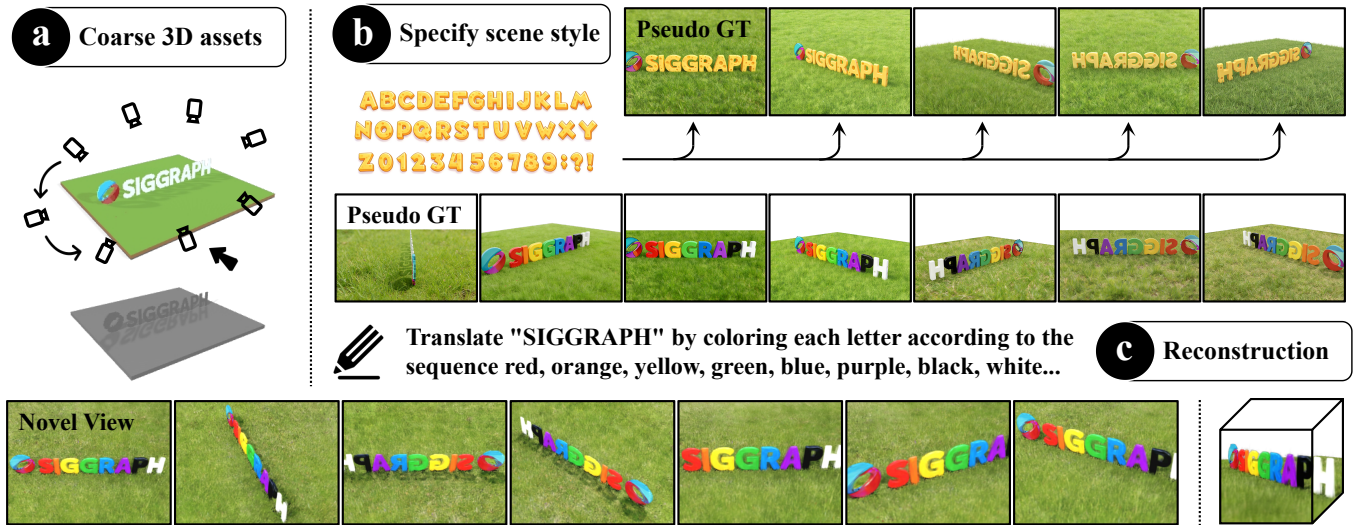


Fig. 1. Overview framework. (a) Users first initialize a coarse geometric scene using manual assembly (e.g., Minecraft) or existing 3D meshes. (b) By specifying the desired visual style via reference images or text prompts, the model generates multi-view pseudo-GTs as supervision. (c) Finally, our method reconstructs a high-quality 3D scene that maintains both style consistency and structural regularity.

3D scene generation is a core technology for gaming, film/VFX, and VR/AR. Growing demand for rapid iteration, high-fidelity detail, and accessible content creation has further increased interest in this area. Existing methods broadly follow two paradigms—indirect 2D-to-3D reconstruction and direct 3D generation—but both are limited by weak structural modeling and heavy reliance on large-scale ground-truth supervision, often producing structural artifacts, geometric inconsistencies, and degraded high-frequency details in complex scenes. We propose GeoDiff3D, an efficient self-supervised framework that uses coarse geometry as a structural anchor and a geometry-constrained 2D diffusion model to provide texture-rich reference images. Importantly, GeoDiff3D does not require strict multi-view consistency of the diffusion-generated references and remains robust to the resulting noisy,

inconsistent guidance. We further introduce voxel-aligned 3D feature aggregation and dual self-supervision to maintain scene coherence and fine details while substantially reducing dependence on labeled data. GeoDiff3D also trains with low computational cost and enables fast, high-quality 3D scene generation. Extensive experiments on challenging scenes show improved generalization and generation quality over existing baselines, offering a practical solution for accessible and efficient 3D scene construction.

CCS Concepts: • **Computing methodologies** → **Reconstruction**.

Additional Key Words and Phrases: 3D Scene Generation, Self-Supervised Optimization, Diffusion Model

1 Introduction

3D scene generation, as a core topic spanning computer graphics, artificial intelligence, and virtual world construction, has garnered significant attention. From open-world creation in games and virtual set construction in films to immersive environments in VR applications, the demand for high-quality 3D scenes continues to grow, with increasing emphasis on rapid iteration, rich visual details, and low barriers to content creation.

*Equal contribution.

[†]Corresponding author. Email: zhangyanju@nju.edu.cn

[‡]Corresponding author. Email: guojie@nju.edu.cn

Authors' Contact Information: Haozhi Zhu, Nanjing University, Nanjing, China, 662024330006@smail.nju.edu.cn; Miaomiao Zhao, Nanjing University, Nanjing, China, 522025330152@smail.nju.edu.cn; Dingyao Liu, Nanjing University, Nanjing, China, 522024330044@smail.nju.edu.cn; Runze Tian, Nanjing University, Nanjing, China, 522024330075@smail.nju.edu.cn; Yan Zhang, Nanjing University, Nanjing, China; Jie Guo, Nanjing University, Nanjing, China; Fenggen Yu, Simon Fraser university, China, yufg1994@gmail.com.

In recent years, diffusion-based generative models have achieved remarkable success in image generation [Ho et al. 2020; Rombach et al. 2022; Saharia et al. 2022] and video generation [Blattmann et al. 2023; Guo et al. 2024; Yang et al. 2024], offering flexible and efficient solutions for visual content creation. Inspired by this progress, plenty of methods [Li et al. 2023; Liu et al. 2024a; Long et al. 2024] have explored reconstructing 3D scenes from multi-view images or videos generated by 2D diffusion models. However, 2D diffusion models excel at producing visual realistic 2D content, but lack explicit constraints and global consistency of 3D structure. In contrast, 3D scene generation requires strict structural coherence and visual consistency. This fundamental mismatch often causes structural artifacts, geometric inconsistencies, and violations of physical constraints in 2D-based reconstruction methods.

Besides, researchers have extended the idea of diffusion models to 3D [Lin et al. 2023; Poole et al. 2022; Tang et al. 2023]. These methods learn 3D generative priors from large-scale 3D datasets and can produce complete 3D outputs from text prompts, sparse views, and even single images. While effective for simple object generation, most existing methods [Chang et al. 2025; Xiang et al. 2025, 2024] struggle to generate complex scenes such as detailed building layouts or large-scale natural environments. This limitation arises from the lack of high quality 3D training data and the complexity of real-world scenes, leading to disorganized structures and blurred details. In summary, whether following an indirect 2D-to-3D reconstruction paradigm or a direct 3D generation paradigm, current methods remain constrained by insufficient modeling of 3D structural priors and a heavy reliance on large training datasets.

Reviewing traditional 3D scene generation pipelines reveals a key insight for addressing these challenges: coarse geometric structures serve as the foundational anchor through the entire modeling process. In conventional workflows, artists first construct rough geometric layouts and then progressively refine textures, lighting, and materials through labor-intensive procedures. Although this process demands substantial expertise and limits rapid iteration, coarse geometry enforces precise spatial constraints, ensuring correct proportions, structural validity, and view consistency. Such geometric anchoring effectively compensates for the lack of explicit 3D structural constraints in existing generative methods and remains indispensable for reliable scene construction.

Meanwhile, despite the difficulty of directly reconstructing complete 3D models from 2D diffusion models, these methods [Li et al. 2023; Liu et al. 2024a; Long et al. 2024] remain highly complementary to coarse geometry. On one hand, 2D diffusion models excel at generating high-quality images with fine-grained local details, which can serve as high-fidelity texture sources without requiring large-scale 3D datasets. On the other hand, their flexibility in visual concept exploration enables efficient style variation and rapid design iteration. Therefore, 2D diffusion models can effectively bridge coarse geometric structures and high-quality 3D scene generation, balancing structural correctness and visual quality.

Based on these observations, we propose a novel framework for high-quality 3D scene generation that integrates coarse geometric constraints with the strengths of 2D diffusion models. Our method avoids complex manual post-processing and heavy reliance on large

annotated datasets. By using coarse geometry as a structural anchor and leveraging diffusion-based image generation for detail synthesis, we introduce a voxel-aligned generative modeling framework that automates texture generation and detail completion. This framework significantly simplifies the 3D scene creation pipeline, offering an efficient and low-barrier alternative to traditional labor-intensive workflows. Fig. 1 illustrates the overall pipeline. As shown in Fig. 1(a), users first construct a coarse geometric scene through manual modeling or asset assembly. Then, as shown in Fig. 1(b), reference images or text prompts are provided to specify the desired visual style. Finally, as shown in Fig. 1(c), our method generates high-quality 3D scenes with both structural coherence and consistent visual appearance.

Specifically, our framework consists of a three-stage progressive pipeline that unifies geometric constraints and realistic details. First, we generate texture reference images. Based on the coarse geometry and the target style, we use 2D diffusion models [Kim et al. 2025; Mou et al. 2023; Zhang et al. 2023] to generate texture-rich yet multi-view inconsistent images, which serve as pseudo-ground-truth (pseudo-GT). Second, we perform 3D feature aggregation and optimization. Inspired by voxel-aligned representations [Jiang et al. 2025; Wang et al. 2025b; Xiang et al. 2024], features extracted from the pseudo-GT images are aligned and aggregated into voxel grids corresponding to the coarse geometry. A sparse 3D decoder then refines the aggregated features and predicts voxel-aligned Gaussian distributions. This volumetric aggregation effectively mitigates floating artifacts and view inconsistency, transferring multi-view information to shared 3D representations before detail synthesis. Third, we introduce a self-supervised training strategy to address the potential multi-view inconsistency of the pseudo-GT. We jointly leverage diffusion-generated reference images, which preserve visual realism, and novel-view renderings from the voxel model, which enforce structural consistency. By designing a tailored set of objective functions, our method effectively balances structural coherence and visual fidelity while significantly reducing reliance on large-scale datasets. Our main contributions include:

- We propose *GeoDiff3D*, a geometry-constrained 2D diffusion-assisted self-supervised framework for 3D scene generation, enabling efficient and high-quality 3D scene creation while effectively addressing the core limitations of existing methods, namely weak structural constraint and heavy dependence on large-scale dataset.
- We introduce a voxel-aligned 3D feature aggregation mechanism that jointly preserves generation quality and structural coherence, reduces over-reliance on reference image consistency, and ensures the completeness of the generated structure.
- We design a dual self-supervised optimization strategy that precisely balances structural consistency and realistic details while significantly reducing reliance on large-scale annotated dataset.
- Our method does not require high-end computational resources and can rapidly generate high-quality 3D scenes, making it well suited for low-barrier, high-efficiency 3D content creation.

2 Related Work

Reconstruction-based 3D Model Creation. In recent years, a class of methods [Gao* et al. 2024; Jiang et al. 2025; Nam et al. 2025; Yu et al. 2024] for building 3D scenes from scratch first generates multi-view images or videos using diffusion models, followed by 3D reconstruction using techniques such as 3D Gaussian Splatting (3DGS) [Kerbl et al. 2023] or NeRF [Mildenhall et al. 2020]. ReconX [Liu et al. 2024a] uses video diffusion models to synthesize video frames as dense input to guide 3DGS optimization. AnySplat [Jiang et al. 2025] leverages camera and depth priors learned from large-scale datasets and directly acquires 3DGS parameters from image features via a feed-forward network. Voyager [Huang et al. 2025] uses depth maps and camera trajectories as constraints to guide the generative model to synthesize videos with explicit spatial logic, further enabling large-scale scene construction through a world cache. Marble [WorldLabs 2025] generates an explorable 3D world from a single image input. However, these methods only optimize in the 2D pixel space and lack explicit 3D geometric guidance, leading to poor multi-view consistency and a disconnect between generation and reconstruction. In contrast, our method uses coarse geometry as a core structural constraint and tightly combines generation and reconstruction through voxel-aligned feature aggregation and a dual self-supervised optimization strategy, ensuring structural consistency while reducing drift and artifacts.

Generation-based 3D Model Creation. Leveraging the strong priors of generative models for 3D reconstruction [Cao et al. 2025; Chen et al. 2024; Liu et al. 2024b; Wu et al. 2024] has become a major research direction. See3D [Ma et al. 2025] is the first to train a 3D generative model directly on large-scale in-the-wild videos without pose annotations, and further supports editing. RomanTex [Feng et al. 2025] injects geometric structure into the attention mechanism of a multi-view diffusion model, improving cross-view texture consistency. ReconViaGen [Chang et al. 2025] combines reconstruction priors from VGGT [Wang et al. 2025a] with diffusion generation priors to enhance controllability. InstantMesh [Xu et al. 2024] combines multi-view diffusion with a sparse reconstruction network to rapidly produce topologically consistent meshes. Despite their impressive progress, most of these methods heavily rely on large-scale annotated 3D datasets and are limited to single-object generation, exhibiting structural degradation and poor generalization in complex scenes. Our method leverages the rich detail generation capability of 2D diffusion models to enhance scene textures, and significantly improves generalization in complex scenes through a dual self-supervised strategy, without requiring massive labeled 3D datasets.

Voxel Representations. Voxel grids, with their regular structure, serve as an effective bridge between 2D visual observations and explicit 3D geometric representations. To address feature alignment, VolSplat [Wang et al. 2025b] constructs a feature-matching cost volume and refines it with 3D U-Net. To improve rendering efficiency, AnySplat [Jiang et al. 2025] introduces Gaussian voxelization, aggregating and filtering Gaussian primitives within voxel grids to significantly reduce redundant computation. UniSplat [Shi et al. 2025] builds a 3D latent scaffold as structural support, enabling flexible capture of time-varying geometry and achieving high-quality

dynamic reconstruction for more complex scenes. Trellis 1.0 [Xiang et al. 2024] introduces a structured latent variable model that compresses complex 3D data into sparse voxel latents and trains a decoder to recover high-fidelity geometry and textures. These works demonstrate the effectiveness of voxel representations for 3D reconstruction. Our method leverages voxels for feature fusion, aligning detailed features generated by 2D diffusion models into 3D space to form a unified representation, balancing structural constraints and visual fidelity.

3 Method

We define the task of *GeoDiff3D* as follows: let M denote a 3D scene model which supports multiple representations such as meshes and voxels, and let a reference image I_{ref} or a text prompt T specify the target visual style. Given these inputs, our goal is to generate a 3D scene represented as 3D Gaussian Splatting (3DGS) [Kerbl et al. 2023] that faithfully preserves the geometry of M while achieving visual consistency with the style of I_{ref} or T .

As illustrated in Fig. 2, GeoDiff3D consists of three stages. First, in the texture reference generation stage, we take the 3D scene model M and camera trajectories as input, extract multi-view projected edge constraints as structural guidance, and combine them with the reference style. Then we use a 2D diffusion model [Kim et al. 2025] to synthesize pseudo-ground-truth (pseudo-GT) texture reference images as guides for the scene generation. Next, in the 3D feature aggregation and optimization stage, the pseudo-GT image features are aligned and aggregated into the voxel grids corresponding to M . A sparse 3D decoder refines these features and predicts voxel-aligned Gaussian distributions to ensure cross-view consistency. Finally, we perform self-supervised optimization using the pseudo-GT images and the rendered images decoded from the second stage, generating a high-quality 3D scene model.

3.1 Texture Reference Image Generation

To achieve high-quality 3D scene reconstruction, we first construct pseudo-GT texture reference images that preserve the scene structure while providing rich style details. This stage combines two complementary cues: the coarse 3D model provides geometric guidance (e.g., contours and depth ordering), while a reference image or text prompt specifies the target style. Leveraging these cues, we use a 2D diffusion model to generate multi-view images. We then select high-quality results as pseudo-GT, which form the foundation for subsequent 3D feature aggregation and scene optimization.

Geometry-Guided Texture Generation. Given predefined camera parameters, the coarse 3D model is first projected into a set of textureless 2D images containing only depth and contour information. Inspired by the anchor-based strategy of VideoFrom3D [Kim et al. 2025], We then employ Flux-ControlNet [XLabs 2024] to inject the extracted line maps as structural priors into the 2D diffusion process, enabling controllable stylized texture synthesis. A reference image or text prompt further specifies the target appearance, including texture characteristics and artistic style. As a result, we obtain multi-view pseudo-GT images with rich textures that are consistent with the reference style.

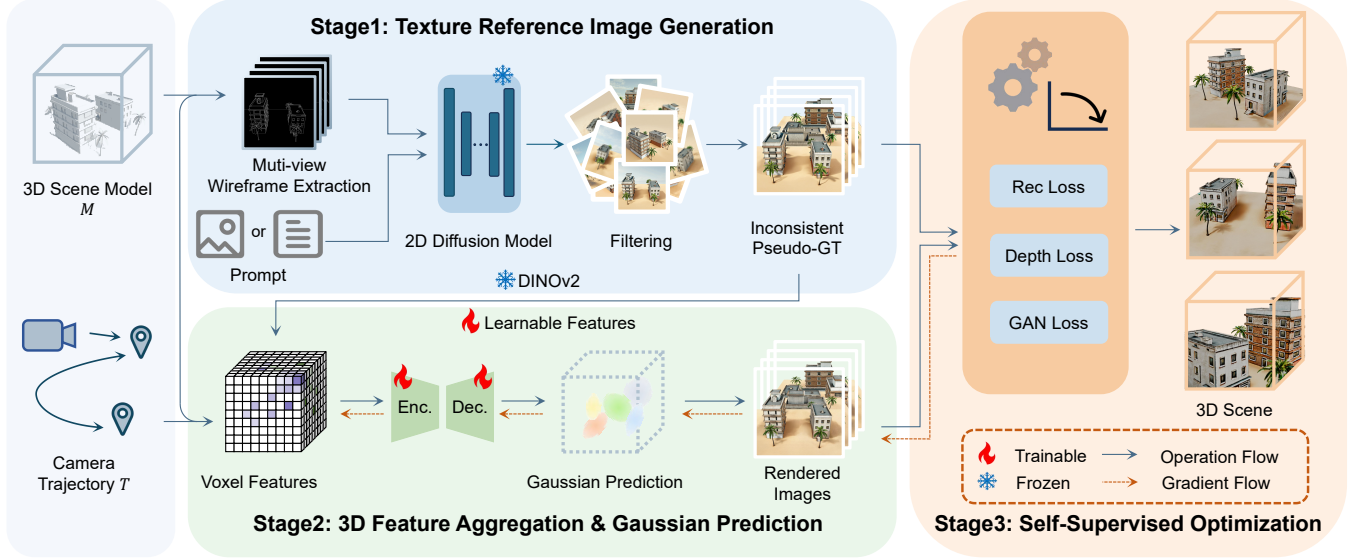


Fig. 2. Overview of GeoDiff3D. In the first stage, we extract structural edges from the input 3D model along the camera trajectory and generate multi-view pseudo-GT images guided by an image diffusion prior. In the second stage, we back-project 2D features from the selected pseudo-GT views into 3D space to form a voxel feature volume, which is then decoded into a 3D Gaussian (3DGS) representation. In the third stage, we perform self-supervised optimization of the generated 3D scene using reconstruction loss, depth loss, and GAN loss.

Multi-Dimensional Quality Filtering Strategy. Although 2D diffusion models bring vivid details, their inherent randomness introduces notable limitations like content hallucination and multi-view inconsistency. To ensure the reliability of pseudo-GT, we design a lightweight filtering strategy to prune the generated images.

First, to prevent off-topic generation, we use CLIP [Radford et al. 2021] to measure the semantic similarity between the generated images and the input reference image or text description and discard low-scoring samples, ensuring that each pseudo-GT faithfully reflects the intended scene semantics and style. Then, we mask the generated images using the textureless 2D projections rendered from the coarse 3D model to filter samples with geometric distortions. Finally, we select a varying number of pseudo-GTs as input based on the size of the scene.

3.2 3D Feature Aggregation and Gaussian Prediction

After obtaining V filtered pseudo-GT images, we could directly apply any 3DGS-based method [Ren et al. 2024; Zhang et al. 2024; Zhu et al. 2023] to reconstruct the scene. However, this suffers from two key limitations: (1) the pseudo-GT generation stage does not explicitly enforce cross-view consistency, leading to geometric distortions such as floating artifacts in 3DGS reconstruction; (2) 3DGS requires a large number of input images, and generating more pseudo-GT images accumulates cross-view inconsistency, further degrading reconstruction quality.

Inspired by voxel-based 3D reconstruction methods [Jiang et al. 2025; Wang et al. 2025b; Xiang et al. 2024], we take the v pseudo-GT images and their camera poses as input, and learn to align and aggregate them into a voxel representation of the coarse geometry.

A sparse 3D decoder then refines the 3D features and predicts voxel-aligned Gaussian distributions.

Feature Extraction and Matching. Given a scene model M , the pseudo-GT image sequence $\{I_v\}_{v=1}^V$ rendered from multiple view-points, and the corresponding camera parameters, we first voxelize the scene into a fixed-resolution sparse 3D voxel grid and extract the occupied voxel set with their indices. For each view I_v , we extract patch-level ViT features F_v using a pretrained DINOv2 [Oquab et al. 2024] encoder. To align 2D semantic information with the 3D voxel space, we project each occupied voxel into each view using the camera intrinsics and extrinsics, and bilinearly sample the corresponding feature from F_v . Finally, we average the voxel features across views to improve robustness to cross-view inconsistency and view-dependent noise, acquiring semantically enriched voxel features.

Feature Refinement. The aggregated voxel feature f_p mainly encodes globally consistent semantics across views. While robust, average aggregating smooths out local high-frequency details, making it insufficient for decoding fine-grained geometry and texture. To address this limitation, we introduce a learnable feature residual $\Delta f_p \in \mathbb{R}^d$ for each occupied voxel and define the refined voxel feature as:

$$\tilde{f}_p = f_p + \Delta f_p, \quad (1)$$

where f_p is the aggregated feature. Δf_p is optimized jointly with the network parameters to adaptively compensate for information lost during aggregation. This design preserves global consistency while restoring local details, enabling accurate and detailed Gaussian parameter decoding in subsequent stages.

Gaussian Prediction. Inspired by the Trellis 1.0 [Xiang et al. 2024] encoder-decoder framework, we employ a sparse 3D VAE to map

the refined voxel features \tilde{f}_p to a renderable Gaussian representation. For each voxel p , the parameters of its j -th Gaussian are defined as

$$\mathbf{g}_{p,j} = (\mathbf{o}_{p,j}, \tilde{\alpha}_{p,j}, \mathbf{s}_{p,j}, \mathbf{q}_{p,j}, \mathbf{c}_{p,j}), j = 1, \dots, 32 \quad (2)$$

where the parameters correspond to the center offset, opacity, scaling, rotation and color, respectively.

To ensure that the predicted parameters lie within valid ranges, we apply bounded mappings: the opacity is constrained to $(0, 1)$ with a Sigmoid function, and the Gaussian center is determined from the voxel center \mathbf{x}_p and the constrained offset. Specifically, set the voxel length as ℓ , the Gaussian center is computed as:

$$\boldsymbol{\mu}_{p,j} = \mathbf{x}_p + \ell \cdot \left(\sigma(\mathbf{o}_{p,j}) - \frac{1}{2} \right), \quad \alpha_{p,j} = \sigma(\tilde{\alpha}_{p,j}), \quad (3)$$

where $\mathbf{o}_{p,j} \in \mathbb{R}^3$ is the center offset predicted by the decoder, and $\sigma(\cdot)$ denotes the Sigmoid function. This parameterization anchors each Gaussian within a local neighborhood aligned with the voxel scale, improving training stability and enforcing alignment with the voxel grid structure.

Deterministic Template Perturbation. With voxel-anchored parameterization, neighboring voxels tend to produce similar offset patterns due to local smoothness. During optimization, Gaussian centers may also be pushed toward the boundaries of the offset range, leading to grid-aligned blocky artifacts in rendering. To alleviate this regularity, we add a deterministic voxel-dependent perturbation to the Gaussian centers:

$$\boldsymbol{\mu}_{p,j} \leftarrow \boldsymbol{\mu}_{p,j} + \rho \cdot \ell \cdot \mathbf{t}_{p,j}, \quad (4)$$

where $\mathbf{t}_{p,j} \in [-1, 1]^3$ is determined from the voxel index and Gaussian number, ρ denotes the perturbation radius. This perturbation weakens strict grid alignment while preserving the global geometry, ensuring more continuous and visually stable renderings.

3.3 Self-Supervised Optimization

After the pipeline described in Sec. 3.2, voxel-rendered images derived from the coarse geometry preserve spatial coherence. However, they are limited by the cross-view inconsistency of pseudo-GT, often leading to blurred details and insufficient realism. Existing voxel-based reconstruction methods [Jiang et al. 2025; Wang et al. 2025b] rely on large-scale annotated 3D datasets for supervised training, which is impractical in the from-scratch reconstruction where such annotations are unavailable.

Inspired by MV2MV [Youcheng Cai 2024], which constructs supervision from complementary pseudo labels, we design a dual-supervision self-supervised optimization strategy. Pseudo-GT from the 2D diffusion model provides realistic visual details, while novel views rendered from the voxel model provide complementary structural consistency. Consistency loss enhances multi-view coherence, and GAN loss preserves high-fidelity visual details. Within this self-supervised framework, we jointly optimize the encoder-decoder network and the learnable voxel feature residuals (Δf_p in Sec. 3.2) in an end-to-end manner. This strategy eliminates the dependence on large-scale annotated 3D data and effectively bridges the gap between 2D diffusion generation and 3D structural requirements, enabling robust and high-quality 3D scene generation. The pipeline is defined as follows:

Consistency Loss. We adopt the standard 3DGS reconstruction loss to supervise the optimization of Gaussians. We render the current Gaussian set to obtain \hat{I}_v for each view, and calculate a weighted combination of pixel-wise L_1 , D -SSIM and LPIPS losses with the corresponding pseudo-GT image I_v . This reconstruction loss suppresses view-dependent noise and appearance drift, thereby improving cross-view consistency and rendering stability. We define the reconstruction loss as follows:

$$\mathcal{L}_{\text{rec}} = \lambda_{L_1} \cdot \mathcal{L}_{L_1} + \lambda_{D\text{-SSIM}} \cdot \mathcal{L}_{D\text{-SSIM}} + \lambda_{LPIPS} \cdot \mathcal{L}_{LPIPS} \quad (5)$$

To further enhance geometric consistency, we introduce patch-based depth regularization [Li et al. 2024] on the depth map d . Specifically, we divide the depth map into separate local patches P , and normalize depth both locally and globally to constrain local depth variations and global shape trends.

$$d_{\text{LN}}(x) = \frac{d(x) - \text{mean}(d(P))}{\text{std}(d(P)) + \epsilon}, \quad (6)$$

$$d_{\text{GN}}(x) = \frac{d(x) - \text{mean}(d(I))}{\text{std}(d(I)) + \epsilon}, \quad (7)$$

where $x \in P$, and I denotes the entire image field. We use \hat{d} for the rendered depth and d^* for the ground-truth depth.

In practice, to avoid numerical instability caused by extremely small variances, we add a stability term ϵ related to the global variance to the denominator. In addition, we use a truncated L_2 norm with a tolerance threshold τ to reduce the influence of noise supervision, where errors are only penalized when they exceed the threshold:

$$\ell_{\tau}(a, b) = \mathbb{I}(|a - b| > \tau) \cdot (a - b)^2. \quad (8)$$

The final depth regularization term is a weighted combination of the local and global term:

$$\mathcal{L}_{\text{depth}} = \lambda_L \mathbb{E}_P [\ell_{\tau}(d_{\text{LN}}, d_{\text{LN}}^*)] + \lambda_G \mathbb{E}_P [\ell_{\tau}(d_{\text{GN}}, d_{\text{GN}}^*)]. \quad (9)$$

GAN Loss. Since pseudo-GT generated by 2D diffusion model inevitably exhibits cross-view inconsistency, relying solely on consistency losses tends to average appearances across views, resulting in over-smoothed and blurry textures. To address this, we introduce adversarial training with a PatchGAN [Isola et al. 2017] discriminator $D(\cdot)$, which enables the model to learn discriminative high-frequency details from pseudo-GT while maintaining global structural consistency.

The discriminator outputs a spatial score map $D(I) \in \mathbb{R}^{H' \times W'}$ for an input image and its mean value is denoted as $\overline{D(I)}$. During adversarial training, high-quality pseudo-GT images generated by the 2D diffusion model are treated as real samples $I \sim p_{\text{data}}$, while images rendered from the current 3D representation are treated as fake samples $\hat{I} \sim p_G$. We adopt a hinge style adversarial loss, and the discriminator target is defined as:

$$\mathcal{L}_D^{\text{GAN}} = \frac{1}{2} \left(\mathbb{E}_{I \sim p_{\text{data}}} \left[\overline{\max(0, 1 - D(I))} \right] + \mathbb{E}_{\hat{I} \sim p_G} \left[\overline{\max(0, 1 + D(\hat{I}))} \right] \right). \quad (10)$$

The generator, including encoder-decoder and the rendering module, has an GAN loss defined as:

$$\mathcal{L}_G^{\text{GAN}} = -\mathbb{E}_{\hat{I} \sim p_G} \left[\overline{D(\hat{I})} \right], \quad (11)$$

We incorporate the GAN and depth losses into the total generator objective with weights λ_{gan} and λ_{depth} , respectively:

$$\mathcal{L}_G = \mathcal{L}_{\text{rec}} + \lambda_{\text{depth}} \cdot \mathcal{L}_{\text{depth}} + \lambda_{\text{gan}} \cdot \mathcal{L}_G^{\text{GAN}} \quad (12)$$

4 Experiments

4.1 Implementation details

In the first-stage of pseudo-GT generation, we generate all pseudo-GT images at a fixed resolution of 1024×1024 . Depending on the scene scale, we use different numbers of pseudo-GT views: 10 – 12 views for large-scale scenes and 4 – 8 views for smaller scenes. During training, we set the voxel grid resolution to 128^3 . The weights of reconstruction-related losses are set following the original 3DGS framework, with the depth loss weight set to 0.1. The GAN loss is assigned a weight of 0.05 and is introduced only after 500 training iterations to avoid disrupting early geometric structure learning, by which time the scene typically already has a relatively stable 3D structure. We employ two separate optimizers for different objectives: one for consistency-related losses with a learning rate of 1×10^{-4} , and another for the GAN loss with a learning rate of 5×10^{-6} . Each scene is trained for 1,000 iterations on a single NVIDIA A800 (40GB) GPU, with a total training time of approximately ten to twenty minutes.

4.2 Model Generation results

Fig. 5 presents qualitative results of our method across diverse scenes. We consider a variety of inputs, including Minecraft-style scenes and untextured scenes. The results in the first two rows demonstrate strong robustness for large-scale outdoor scenes: even with complex spatial layouts and rich environmental details, our method achieves high visual quality with well-preserved fine details. The last two rows highlight consistently stable performance on buildings-centric scenes, where complex geometric structures such as fine contours and multi-component assemblies are faithfully reconstructed, generating high-fidelity scene models that accurately capture architectural characteristics. These results clearly demonstrate the adaptability of our method across different scene types. In addition, Fig. 8 illustrates the fine-grained style controllability of our method with different modifier prompts, further validating its flexibility, efficiency, and scalability for style control. Additional results are provided in the supplementary material.

4.3 Baseline Comparisons

Qualitative Comparisons. To assess the efficacy of our method, we conduct comparative experiments against five representative methods, including the image-based generative method Trellis 1.0 [Xiang et al. 2024], the world models World-Mirror [Liu et al. 2025] and Marble [WorldLabs 2025], the 3D geometry constrained video synthesis method VideoFrom3D [Kim et al. 2025], and the sparse-view 3DGS reconstruction method FSGS [Zhu et al. 2023].

The experimental settings are as follows. For Trellis 1.0, we treat the existing sparse voxel representation as the sparse structural prediction from its first stage and feed multi-view pseudo-GT images into its second-stage generation module. For World-Mirror, we provide camera poses and ground-truth depth as prior information. For Marble in indoor scenes, we import an existing indoor model

Table 1. Quantitative comparisons with Trellis 1.0 [Xiang et al. 2024], World-Mirror [Liu et al. 2025], FSGS [Zhu et al. 2023] and VF3D [Kim et al. 2025].

Method	PSNR-D \uparrow	MUSIQ \uparrow	MANIQ \uparrow	CC \uparrow	CS \uparrow
Trellis 1.0	17.41	44.71	0.26	0.92	0.81
World-Mirror	15.09	50.76	0.25	0.90	0.76
FSGS	18.26	57.07	0.31	0.90	0.84
VF3D+3DGS	17.46	48.73	0.27	0.85	0.86
Ours	20.39	58.06	0.35	0.93	0.90

Table 2. Quantitative comparisons with Marble [WorldLabs 2025].

Method	PSNR-D \uparrow	MUSIQ \uparrow	MANIQ \uparrow	CC \uparrow	CS \uparrow
Marble	16.68	55.75	0.35	0.90	0.82
Ours	20.39	58.06	0.35	0.93	0.90

into its indoor pipeline and perform 3D generation conditioned on style descriptions derived from reference images. Since Marble relies on panoramic inputs for outdoor scenes and is not applicable to the inconsistent pseudo-GT setting in our framework, we report comparisons with Marble only on indoor scenes. For VideoFrom3D, we incorporate our pseudo-GT as anchor points in the video generation and reconstruct 3D scenes using 3DGS based on its synthesized video outputs. For FSGS, we use the pseudo-GT images from our first stage as input, and initialize the COLMAP point cloud with our densified sparse voxel points.

Fig. 7 shows qualitative comparisons against the baseline methods. Due to the limited geometric controllability of generative models, Trellis 1.0 often fails to preserve the original geometry when conditioned on existing 3D structures. Traditional 3DGS reconstruction based on VideoFrom3D outputs and FSGS often suffer from needle-like artifacts and blurred details caused by view inconsistency. World-Mirror relies on a VGGT [Wang et al. 2025a] like prediction framework, where accurate geometric reconstruction becomes challenging when the inputs are inconsistent. In Fig. 6, we show a separate comparison with Marble (indoor), which, similar to Trellis 1.0, often fails to preserve the input geometry. In contrast, our method effectively avoids these issues and consistently achieves superior visual quality and higher structural fidelity, even under complex scene conditions.

Quantitative Comparisons. For the test dataset, we construct 12 3D scene models, including several scenes from Minecraft assets and manually created white-mesh scenes. The white-mesh assets are collected from open asset platforms such as TurboSquid [TurboSquid 2026] and Free3D [Free3D 2026]. The dataset consists of three indoor scenes, four buildings-centric scenes and five landscape scenes. For each scene, we select two different text or style prompts, constructing a total of 24 test cases. To evaluate our method against the baseline methods, we randomly sample 8 or 16 camera viewpoints per scene and report the following evaluation metrics.

For visual quality comparison, we use MUSIQ [Ke et al. 2021] and MANIQA [Yang et al. 2022], which measure texture sharpness and perceptual realism from a human visual perspective. For geometric

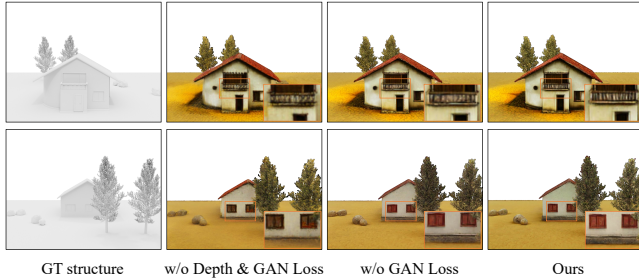


Fig. 3. Qualitative results on the effectiveness of our self-supervised optimization strategy. Orange boxes indicate the same regions of the input geometry.

Table 3. Quantitative comparison of different optimization strategies.

Method	PSNR-D \uparrow	MUSIQ \uparrow	MANIQ \uparrow	CC \uparrow
w/o Depth & GAN Loss	12.67	34.74	0.29	0.88
w/o GAN Loss	14.67	40.31	0.30	0.89
Ours	19.00	57.08	0.33	0.93

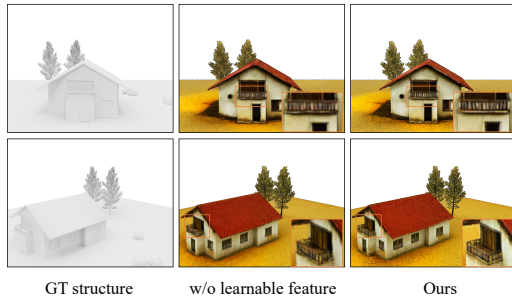


Fig. 4. Qualitative results with and without the learnable features. Orange boxes indicate the same regions of the input geometry.

Table 4. Quantitative comparison of the impact of the learnable features.

Method	PSNR-D \uparrow	MUSIQ \uparrow	MANIQ \uparrow	CC \uparrow
w/o learnable feature	17.82	45.55	0.31	0.92
Ours	19.00	57.08	0.33	0.93

consistency, we adopt PSNR-D, which measures the PSNR between ground-truth depth maps and depth maps estimated from rendered images using a monocular depth estimator. For style consistency, following WonderWorld [Yu et al. 2025], we compute the CLIP score between each rendered image and its corresponding pseudo-GT, and the cosine similarity between the CLIP embeddings of each novel view and the corresponding center view. Tabs. 1 and 2 shows quantitative comparisons with the baselines, indicating that our method consistently achieves better visual quality and stronger geometric consistency.

4.4 Ablation Study

Effectiveness of Self-Supervised Optimization. We further investigate the effectiveness of our self-supervised optimization strategy through three ablation studies, as shown in Fig. 3, which evaluate the impact of the depth loss, the GAN loss, and their joint supervision. Removing both the depth and GAN losses and relying solely on the consistency loss (the second column of Fig. 3) leads to noticeable structural artifacts, broken multi-view continuity, and blurred details, due to the lack of explicit structural constraints and detail refinement. Removing only the GAN loss (the third column of Fig. 3) significantly improves the structural coherence of the scene but results in insufficient visual richness and texture fidelity. Using the full self-supervised optimization strategy (the fourth column of Fig. 3) effectively balances structural regularity and visual richness. The quantitative results reported in Tab. 3 further demonstrate the effectiveness of the strategies we proposed.

Effectiveness of Learnable Features. The initial voxel features are obtained by back-projecting and then averaging multi-view features. While this process alleviates cross-view inconsistencies, it also weakens the representation of local high-frequency information. The qualitative results in Fig. 4 demonstrate the effectiveness of the proposed learnable features: the reconstructed balcony railings are noticeably clearer across multiple viewpoints, exhibiting richer geometric and texture details. This improvement arises because the learnable features are continuously updated during training, enabling the model to adaptively capture and recover missing local details. The quantitative results reported in Tab. 4 further support this observation, showing consistent improvements across multiple reconstruction quality metrics. Together, these results confirm the crucial role of learnable features in enhancing detail recovery and overall reconstruction quality, achieving a smooth transition from coarse-grained to fine-grained 3D reconstruction. See the supplementary material for more ablation experiments.

5 Conclusion

We propose GeoDiff3D, a geometry-guided generative framework that leverages coarse geometry as a structural anchor and diffusion models as a strong prior for detail synthesis to efficiently generate high-quality 3D scenes. Through three stages—texture reference image generation, voxel-aligned 3D feature aggregation, and self-supervised optimization—our framework effectively exploits the structural anchoring of coarse geometry and the rich detail generation capability of 2D diffusion models. The voxel-aligned mechanism and self-supervised strategy effectively balance structural coherence and visual fidelity, while significantly reducing reliance on large-scale labeled data and extensive computational resources. Extensive experiments demonstrate that GeoDiff3D achieves robust performance on complex scenes, outperforming existing baselines in both generation quality and adaptability, providing a low-barrier and efficient solution for practical 3D scene construction.

Limitations. Our method does not explicitly model geometry-free regions, which limits the realism of sky and atmospheric effects. Moreover, using line-drawing cues as diffusion priors cannot capture continuous depth changes, weak textures, or complex occlusions,

making pseudo-GT guidance unreliable in challenging cases. Future work will explore explicit sky/background modeling and richer geometric cues (e.g., depth/normal/semantic signals) to improve robustness. More detailed information can be found in the supplementary material.

References

- Andreas Blattmann, Tim Dockhorn, Sumith Kulal, Daniel Mendelevitch, Maciej Kilian, Dominik Lorenz, Yam Levi, Zion English, Vikram Voleti, Adam Letts, Varun Jampani, and Robin Rombach. 2023. Stable Video Diffusion: Scaling Latent Video Diffusion Models to Large Datasets. arXiv:2311.15127 [cs.CV] <https://arxiv.org/abs/2311.15127>
- Chenjie Cao, Jingkai Zhou, shikai Li, Jingyun Liang, Chaohui Yu, Fan Wang, Xiangyang Xue, and Yanwei Fu. 2025. Uni3C: Unifying Precisely 3D-Enhanced Camera and Human Motion Controls for Video Generation. *arXiv preprint arXiv:2504.14899* (2025).
- Jiahao Chang, Chongjie Ye, Yushuang Wu, Yuantao Chen, Yidan Zhang, Zhongjin Luo, Chenghong Li, Yihao Zhi, and Xiaoguang Han. 2025. ReconViaGen: Towards Accurate Multi-view 3D Object Reconstruction via Generation. *arXiv preprint arXiv:2510.23306* (2025).
- Yuedong Chen, Chuanxia Zheng, Haofei Xu, Bohan Zhuang, Andrea Vedaldi, Tat-Jen Cham, and Jianfei Cai. 2024. NvSplat360: Feed-forward 360 scene synthesis from sparse views. *Advances in Neural Information Processing Systems* 37 (2024), 107064–107086.
- Yifei Feng, Mingxin Yang, Shuhui Yang, Sheng Zhang, Jiaao Yu, Zibo Zhao, Yuhong Liu, Jie Jiang, and Chunchao Guo. 2025. RomanTex: Decoupling 3D-aware Rotary Positional Embedded Multi-Attention Network for Texture Synthesis. In *Proceedings of the IEEE/CVF International Conference on Computer Vision (ICCV)*, 17203–17213.
- Free3D. 2026. Free3D: Free 3D Models. <https://free3d.com/>. Accessed: 2026-01-22.
- Ruiqi Gao*, Aleksander Holynski*, Philipp Henzler, Arthur Brussee, Ricardo Martin-Brualla, Pratul P. Srinivasan, Jonathan T. Barron, and Ben Poole*. 2024. CAT3D: Create Anything in 3D with Multi-View Diffusion Models. *Advances in Neural Information Processing Systems* (2024).
- Yuwei Guo, Ceyuan Yang, Anyi Rao, Zhengyang Liang, Yaohui Wang, Yu Qiao, Maneesh Agrawala, Dahua Lin, and Bo Dai. 2024. AnimateDiff: Animate Your Personalized Text-to-Image Diffusion Models without Specific Tuning. *International Conference on Learning Representations* (2024).
- Jonathan Ho, Ajay Jain, and Pieter Abbeel. 2020. Denoising Diffusion Probabilistic Models. In *Advances in Neural Information Processing Systems*, H. Larochelle, M. Ranzato, R. Hadsell, M.F. Balcan, and H. Lin (Eds.), Vol. 33. Curran Associates, Inc., 6840–6851. https://proceedings.neurips.cc/paper_files/paper/2020/file/4c5bfc9e8584af0d967f1ab10179ca4b-Paper.pdf
- Tianyu Huang, Wangguandong Zheng, Tengfei Wang, Yuhao Liu, Zhenwei Wang, Junta Wu, Jie Jiang, Hui Li, Rynson WH Lau, Wangmeng Zuo, and Chunchao Guo. 2025. Voyager: Long-Range and World-Consistent Video Diffusion for Explorable 3D Scene Generation. *arXiv preprint arXiv:2506.04225* (2025).
- Phillip Isola, Jun-Yan Zhu, Tinghui Zhou, and Alexei A. Efros. 2017. Image-To-Image Translation With Conditional Adversarial Networks. In *Proceedings of the IEEE Conference on Computer Vision and Pattern Recognition (CVPR)*.
- Lihan Jiang, Yucheng Mao, Linning Xu, Tao Lu, Kerui Ren, Yichen Jin, Xudong Xu, Mulin Yu, Jiangmiao Pang, Feng Zhao, et al. 2025. Anysplat: Feed-forward 3d gaussian splatting from unconstrained views. *ACM Transactions on Graphics (TOG)* 44, 6 (2025), 1–16.
- Junjie Ke, Qifei Wang, Yilin Wang, Peyman Milanfar, and Feng Yang. 2021. MUSIQ: Multi-Scale Image Quality Transformer. In *Proceedings of the IEEE/CVF International Conference on Computer Vision (ICCV)*, 5148–5157.
- Bernhard Kerbl, Georgios Kopanas, Thomas Leimkühler, and George Drettakis. 2023. 3D Gaussian Splatting for Real-Time Radiance Field Rendering. *ACM Transactions on Graphics* 42, 4 (July 2023).
- Geonung Kim, Janghyeok Han, and Sunghyun Cho. 2025. VideoFrom3D: 3D Scene Video Generation via Complementary Image and Video Diffusion Models. In *SIGGRAPH Asia 2025 Conference Papers (SA Conference Papers '25)*. ACM, Hong Kong, Hong Kong, 1–11. doi:10.1145/3757377.3763871
- Jiahao Li, Hao Tan, Kai Zhang, Zexiang Xu, Fujun Luan, Yinghao Xu, Yicong Hong, Kalyan Sunkavalli, Greg Shakhnarovich, and Sai Bi. 2023. Instant3D: Fast Text-to-3D with Sparse-View Generation and Large Reconstruction Model. <https://arxiv.org/abs/2311.06214> (2023).
- Jiahe Li, Jiawei Zhang, Xiao Bai, Jin Zheng, Xin Ning, Jun Zhou, and Lin Gu. 2024. DNGaussian: Optimizing Sparse-View 3D Gaussian Radiance Fields with Global-Local Depth Normalization. *arXiv preprint arXiv:2403.06912* (2024).
- Chen-Hsuan Lin, Jun Gao, Luming Tang, Towaki Takikawa, Xiaohei Zeng, Xun Huang, Karsten Kreis, Sanja Fidler, Ming-Yu Liu, and Tsung-Yi Lin. 2023. Magic3D: High-Resolution Text-to-3D Content Creation. In *Proceedings of the IEEE/CVF Conference on Computer Vision and Pattern Recognition (CVPR)*, 300–309.
- Fangfu Liu, Wenjiang Sun, Hanyang Wang, Yikai Wang, Haowen Sun, Junliang Ye, Jun Zhang, and Yueqi Duan. 2024a. ReconX: Reconstruct Any Scene from Sparse Views with Video Diffusion Model. arXiv:2408.16767 [cs.CV] <https://arxiv.org/abs/2408.16767>
- Xi Liu, Chaoyi Zhou, and Siyu Huang. 2024b. 3DGS-Enhancer: Enhancing Unbounded 3D Gaussian Splatting with View-Consistent 2D Diffusion Priors. In *Advances in Neural Information Processing Systems (NeurIPS)*.
- Yifan Liu, Zhiyuan Min, Zhenwei Wang, Junta Wu, Tengfei Wang, Yixuan Yuan, Yawei Luo, and Chunchao Guo. 2025. WorldMirror: Universal 3D World Reconstruction with Any-Prior Prompting. *arXiv preprint arXiv:2510.10726* (2025).
- Xiaoxiao Long, Yuan-Chen Guo, Cheng Lin, Yuan Liu, Zhiyang Dou, Lingjie Liu, Yuexin Ma, Song-Hai Zhang, Marc Habermann, Christian Theobalt, and Wenping Wang. 2024. Wonder3D: Single Image to 3D using Cross-Domain Diffusion. In *Proceedings of the IEEE/CVF Conference on Computer Vision and Pattern Recognition (CVPR)*, 9970–9980.
- Baorui Ma, Huachen Gao, Haoge Deng, Zhengxiong Luo, Tiejun Huang, Lulu Tang, and Xinlong Wang. 2025. You See it, You Got it: Learning 3D Creation on Pose-Free Videos at Scale. In *IEEE/CVF conference on computer vision and pattern recognition*.
- Ben Mildenhall, Pratul P. Srinivasan, Matthew Tancik, Jonathan T. Barron, Ravi Ramamoorthi, and Ren Ng. 2020. NeRF: Representing Scenes as Neural Radiance Fields for View Synthesis. In *ECCV*.
- Chong Mou, Xintao Wang, Liangbin Xie, Yanze Wu, Jian Zhang, Zhongang Qi, Ying Shan, and Xiaoohu Qie. 2023. T2i-adapter: Learning adapters to dig out more controllable ability for text-to-image diffusion models. *arXiv preprint arXiv:2302.08453* (2023).
- Hyeongjin Nam, Donghwan Kim, Gyeongsik Moon, and Kyoung Mu Lee. 2025. PARTE: Part-Guided Texturing for 3D Human Reconstruction from a Single Image. In *Proceedings of the IEEE/CVF International Conference on Computer Vision (ICCV)*, 8547–8557.
- Maxime Oquab, Timothée Darcet, Théo Moutakanni, Huy Vo, Marc Szafraniec, Vasil Khalidov, Pierre Fernandez, Daniel Haziza, Francisco Massa, Alaaeldin El-Nouby, Mahmoud Assran, Nicolas Ballas, Wojciech Galuba, Russell Howes, Po-Yao Huang, Shang-Wen Li, Ishan Misra, Michael Rabbat, Vasu Sharma, Gabriel Synnaeve, Hu Xu, Hervé Jegou, Julien Mairal, Patrick Labatut, Armand Joulin, and Piotr Bojanowski. 2024. DINOv2: Learning Robust Visual Features without Supervision. arXiv:2304.07193 [cs.CV] <https://arxiv.org/abs/2304.07193>
- Ben Poole, Ajay Jain, Jonathan T. Barron, and Ben Mildenhall. 2022. DreamFusion: Text-to-3D using 2D Diffusion. arXiv:2209.14988 [cs.CV] <https://arxiv.org/abs/2209.14988>
- Alec Radford, Jong Wook Kim, Chris Hallacy, Aditya Ramesh, Gabriel Goh, Sandhini Agarwal, Girish Sastry, Amanda Askell, Pamela Mishkin, Jack Clark, Gretchen Krueger, and Ilya Sutskever. 2021. Learning Transferable Visual Models From Natural Language Supervision. arXiv:2103.00020 [cs.CV] <https://arxiv.org/abs/2103.00020>
- Kerui Ren, Lihan Jiang, Tao Lu, Mulin Yu, Linning Xu, Zhangkai Ni, and Bo Dai. 2024. Octree-gs: Towards consistent real-time rendering with lod-structured 3d gaussians. *arXiv preprint arXiv:2403.17898* (2024).
- Robin Rombach, Andreas Blattmann, Dominik Lorenz, Patrick Esser, and Björn Ommer. 2022. High-Resolution Image Synthesis With Latent Diffusion Models. In *Proceedings of the IEEE/CVF Conference on Computer Vision and Pattern Recognition (CVPR)*, 10684–10695.
- Chitwan Saharia, William Chan, Saurabh Saxena, Lala Li, Jay Whang, Emily L Denton, Kamyar Ghasemipour, Raphael Gontijo Lopes, Burcu Karagol Ayan, Tim Salimans, Jonathan Ho, David J Fleet, and Mohammad Norouzi. 2022. Photorealistic Text-to-Image Diffusion Models with Deep Language Understanding. In *Advances in Neural Information Processing Systems*, S. Koyejo, S. Mohamed, A. Agarwal, D. Belgrave, K. Cho, and A. Oh (Eds.), Vol. 35. Curran Associates, Inc., 36479–36494. https://proceedings.neurips.cc/paper_files/paper/2022/file/ec795aeade0b7d230fa35cbaf04c041-Paper-Conference.pdf
- Chen Shi, Shaoshuai Shi, Xiaoyang Lyu, Chunyang Liu, Kehua Sheng, Bo Zhang, and Li Jiang. 2025. UniSplat: Unified Spatio-Temporal Fusion via 3D Latent Scaffolds for Dynamic Driving Scene Reconstruction. *arXiv preprint arXiv:2511.04595* (2025).
- Junshu Tang, Tengfei Wang, Bo Zhang, Ting Zhang, Ran Yi, Lizhuo Ma, and Dong Chen. 2023. Make-It-3D: High-fidelity 3D Creation from A Single Image with Diffusion Prior. In *Proceedings of the IEEE/CVF International Conference on Computer Vision (ICCV)*, 22819–22829.
- TurboSquid. 2026. TurboSquid 3D Models Marketplace. <https://www.turbosquid.com/>. Accessed: 2026-01-22.
- Jianyuan Wang, Minghao Chen, Nikita Karaev, Andrea Vedaldi, Christian Rupprecht, and David Novotny. 2025a. VGGT: Visual Geometry Grounded Transformer. In *Proceedings of the IEEE/CVF Conference on Computer Vision and Pattern Recognition (CVPR)*, 5294–5306.
- Weijie Wang, Yeqing Chen, Zeyu Zhang, Hengyu Liu, Haoxiao Wang, Zhiyuan Feng, Wenkang Qin, Zheng Zhu, Donny Y. Chen, and Bohan Zhuang. 2025b. VolSplat: Rethinking Feed-Forward 3D Gaussian Splatting with Voxel-Aligned Prediction. *arXiv preprint arXiv:2509.19297* (2025).
- WorldLabs. 2025. Marble: A Multimodal World Model. <https://marble.worldlabs.ai/>.

- Rundi Wu, Ben Mildenhall, Philipp Henzler, Keunhong Park, Ruiqi Gao, Daniel Watson, Pratul P. Srinivasan, Dor Verbin, Jonathan T. Barron, Ben Poole, and Aleksander Ho?y?ski. 2024. ReconFusion: 3D Reconstruction with Diffusion Priors. In *Proceedings of the IEEE/CVF Conference on Computer Vision and Pattern Recognition (CVPR)*. 21551–21561.
- Jianfeng Xiang, Xiaoxue Chen, Sicheng Xu, Ruicheng Wang, Zelong Lv, Yu Deng, Hongyuan Zhu, Yue Dong, Hao Zhao, Nicholas Jing Yuan, and Jiaolong Yang. 2025. Native and Compact Structured Latents for 3D Generation. *Tech report* (2025).
- Jianfeng Xiang, Zelong Lv, Sicheng Xu, Yu Deng, Ruicheng Wang, Bowen Zhang, Dong Chen, Xin Tong, and Jiaolong Yang. 2024. Structured 3D Latents for Scalable and Versatile 3D Generation. *arXiv preprint arXiv:2412.01506* (2024).
- XLabs. 2024. x-flux. <https://github.com/XLabs-AI/x-flux>
- Jiale Xu, Weihao Cheng, Yiming Gao, Xintao Wang, Shenghua Gao, and Ying Shan. 2024. InstantMesh: Efficient 3D Mesh Generation from a Single Image with Sparse-view Large Reconstruction Models. *arXiv preprint arXiv:2404.07191* (2024).
- Sidi Yang, Tianhe Wu, Shuwei Shi, Shanshan Lao, Yuan Gong, Mingdeng Cao, Jiahao Wang, and Yujiu Yang. 2022. MANIQA: Multi-Dimension Attention Network for No-Reference Image Quality Assessment. In *Proceedings of the IEEE/CVF Conference on Computer Vision and Pattern Recognition (CVPR) Workshops*. 1191–1200.
- Zhuoyi Yang, Jiayan Teng, Wendi Zheng, Ming Ding, Shiyu Huang, Jiazheng Xu, Yuanming Yang, Wenyi Hong, Xiaohan Zhang, Guanyu Feng, et al. 2024. CogVideoX: Text-to-Video Diffusion Models with An Expert Transformer. *arXiv preprint arXiv:2408.06072* (2024).
- Ligang Liu Youcheng Cai, Runshi Li. 2024. MV2MV: Multi-View Image Translation via View-Consistent Diffusion Models. *ACM Transactions on Graphics (SIGGRAPH Asia 2024)* 43, 6 (2024).
- Hong-Xing Yu, Haoyi Duan, Charles Herrmann, William T. Freeman, and Jiajun Wu. 2025. WonderWorld: Interactive 3D Scene Generation from a Single Image. In *Proceedings of the IEEE/CVF Conference on Computer Vision and Pattern Recognition (CVPR)*. 5916–5926.
- Wangbo Yu, Jinbo Xing, Li Yuan, Wenbo Hu, Xiaoyu Li, Zhipeng Huang, Xiangjun Gao, Tien-Tsin Wong, Ying Shan, and Yonghong Tian. 2024. ViewCrafter: Taming Video Diffusion Models for High-fidelity Novel View Synthesis. *arXiv preprint arXiv:2409.02048* (2024).
- Lvmin Zhang, Anyi Rao, and Maneesh Agrawala. 2023. Adding Conditional Control to Text-to-Image Diffusion Models.
- Zheng Zhang, Wenbo Hu, Yixing Lao, Tong He, and Hengshuang Zhao. 2024. Pixel-GS: Density Control with Pixel-aware Gradient for 3D Gaussian Splatting. In *ECCV*.
- Zehao Zhu, Zhiwen Fan, Yifan Jiang, and Zhangyang Wang. 2023. FSGS: Real-Time Few-Shot View Synthesis using Gaussian Splatting. arXiv:2312.00451 [cs.CV]



Fig. 5. Qualitative results across various scenes. The first column presents the inputs, including the style reference (top-left) and the text prompt (bottom-left). The second column shows representative pseudo-GT images generated by our method. The remaining images show our renderings from different viewpoints.

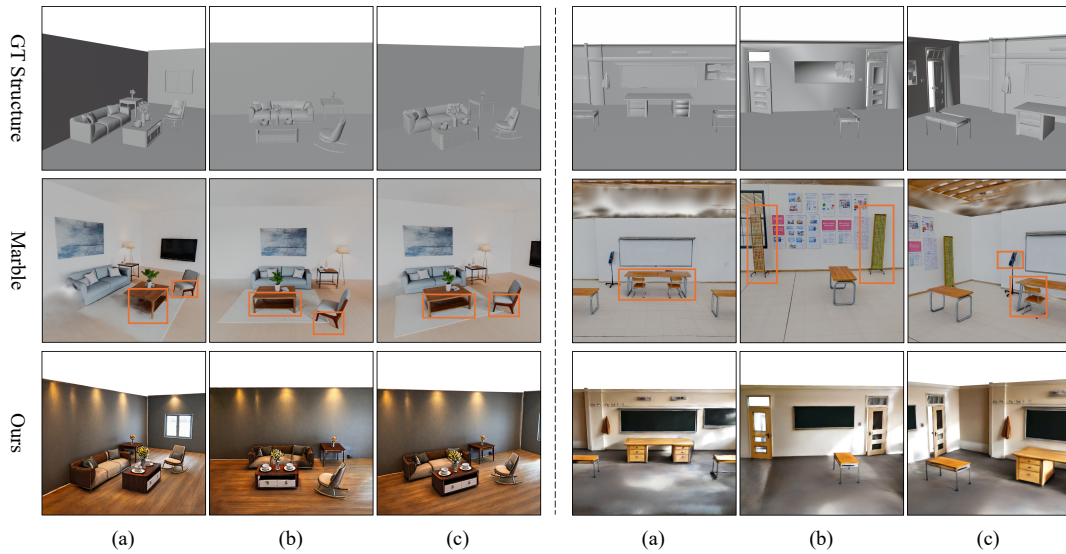


Fig. 6. Qualitative comparisons with Marble [WorldLabs 2025] (indoor pipeline). Orange boxes highlight Marble’s geometric deviations.

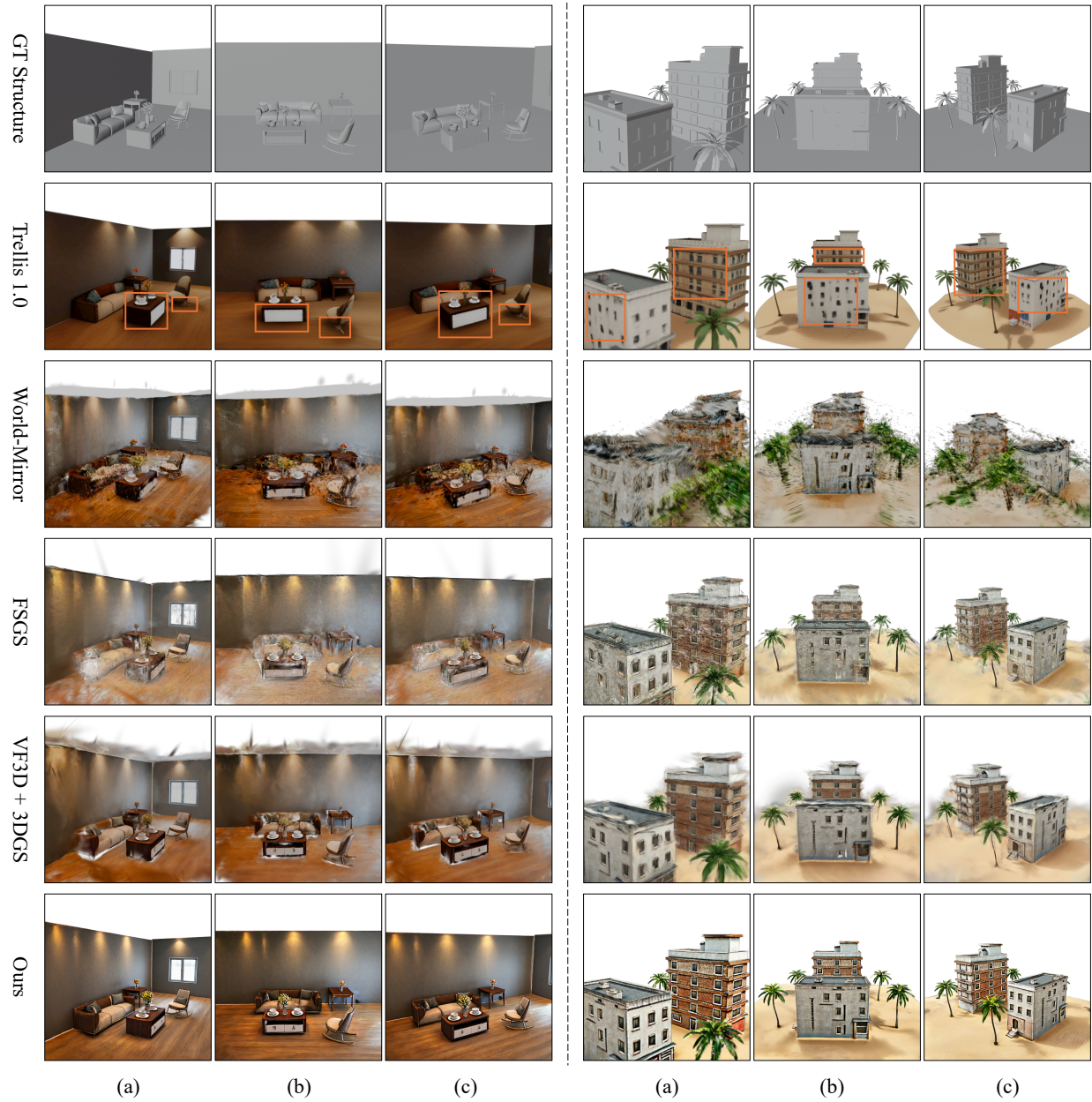


Fig. 7. Qualitative comparisons with Trellis 1.0 [Xiang et al. 2024], World-Mirror [Huang et al. 2025], FSGS [Zhu et al. 2023], and VideoFrom3D [Kim et al. 2025] (3DGS reconstructions from synthesized videos). Orange boxes highlight Trellis 1.0’s geometric deviations.



Fig. 8. Seasonal style transfer on the same scene. Given different style references, our method can switch the scene’s appearance (e.g., four seasons) while preserving its geometry.